Slow electron velocity-map imaging photoelectron spectra of the methoxide anion

Matthew J. Nee, Andreas Osterwalder,[a] Jia Zhou, and Daniel M. Neumark[b]
Department of Chemistry, University of California, Berkeley, California 94720 and Chemical Sciences Division, Lawrence Berkeley Laboratory, Berkeley, California 94720

(Received 20 March 2006; accepted 16 May 2006; published online 5 July 2006)

High resolution anion photodetachment spectra are presented for the methoxide anion and its fully deuterated counterpart. The spectra were obtained with slow electron velocity-map imaging. Improved electron affinities are determined for CH_3O as 1.5690 ± 0.0019 eV and for CD_3O as 1.5546 ± 0.0019 eV. The spectra resolve many features associated with spin-orbit and vibronic coupling that were not seen in previous photodetachment studies. Photoelectron angular distributions taken as a function of detachment wavelength for the ground vibronic state transitions are recorded and are consistent with the removal of a nonbonding, *p*-type electron localized on the oxygen atom. Several hot bands and sequence bands are observed for the first time, providing insight into the vibrational structure of the methoxide anion. The results are compared to recent calculations of the anion photoelectron spectra that incorporate bilinear coupling terms among the methoxy vibrational modes and are found to be in reasonable agreement. © *2006 American Institute of Physics*. [DOI: 10.1063/1.2212411]

I. INTRODUCTION

Many alkoxy radicals, $C_nH_{2n+1}O$, play an important role in a variety of combustion[1] and atmospheric reactions.[2] Despite considerable experimental and theoretical efforts, even the simplest of this class, the methoxy radical (CH_3O), is not fully understood and remains actively studied. The methoxy radical is a highly reactive species with an unusually complicated vibronic structure. Because of its degenerate ground electronic state, methoxy is subject to Jahn-Teller effects. In addition, the open-shell structure enables spin-orbit interactions that further lift the degeneracy of the vibronic states. The small size of the methoxy radical makes it particularly appealing for modeling the interplay between these two effects. We present high resolution photodetachment spectra for both CH_3O and CD_3O. Using the slow electron velocity-map imaging[3] (SEVI) apparatus recently developed in our laboratory, we are able to resolve and assign structures which were not seen in earlier photoelectron (PE) spectra.

The methoxy and ethoxy radicals were first observed[4] in 1953 in the fluorescence spectrum obtained upon UV excitation of ethyl nitrate vapor. Since then, numerous studies, including electronic absorption,[5] PE spectroscopy,[6–8] infrared spectroscopy,[9] laser induced fluorescence (LIF),[10–14] emission spectroscopy,[15,16] stimulated emission pumping (SEP),[17,18] and photodissociation,[19,20] have provided considerable information regarding the vibronic (and, in some cases, rovibronic) structure of methoxy and its deuterated counterpart. Within C_{3v} symmetry, methoxy has three totally symmetric and three (twofold degenerate) non-totally symmetric modes. These modes, including their vibrational symmetry, are summarized in Table I. Much of the early experimental work was summarized in 1989 by Foster and Miller.[12] Despite sustained interest, the unambiguous experimental confirmation of the presence of spin-orbit and Jahn-Teller effects was not provided until 1986 when Brossard *et al.* monitored emission in the $\tilde{A}(^2A_1) \rightarrow \tilde{X}(^2E)$ electronic transitions and assigned several vibrational frequencies.[16] More recent work, including exhaustive assignments to jet-cooled SEP (Refs. 17 and 18) and LIF (Refs. 11, 13, and 14) spectra, has progressively improved the assignment of the rovibronic structure of methoxy, although some discrepancies are found regarding the assignment of the various optical spectra.

The first PE spectrum of the methoxide anion was acquired by Engelking *et al.* in 1978.[6] The electron affinities (EAs) determined by this and susbsequent PE work are collected in Table II. The simple appearance of the spectra of both CH_3O^- and CD_3O^- led the authors to assign the observed peaks to a progression in the totally symmetric ν_2 (H-atom umbrella) mode of the radical, an assignment that was later revised in higher resolution PE spectra by Osborn *et al.*[7] and Ramond *et al.*[8] These more recent spectra, taken with an energy resolution of approximately 10 meV (80 cm^{-1}), demonstrated that many features in the original PE spectrum were composed of at least two peaks that were generally split by far more than the 62 cm^{-1} ground state spin-orbit splitting determined by Brossard *et al.*[16] and were thus due to closely spaced vibrational levels of the radical. Based on comparison with the SEP spectra,[17] all progressions in the PE spectra were assigned to non-totally symmetric vibrational modes, an unusual result for a measurement of this type. Although essentially no experimental information appears regarding the anion frequencies, early calculations[21] indicated that the ejected electron is removed from a non-

[a]Present address: Fritz-Haber-Institut der Max-Planck-Gesellschaft, Faradayweg 4-6, 14195 Berlin, Germany.
[b]Author to whom correspondence should be addressed. Electronic mail: dneumark@berkeley.edu

TABLE I. Vibrational modes of the methoxy radical within C_{3v} symmetry, and the vibronic levels including the Jahn-Teller (JT) interaction. Fundamental frequencies taken from Ref. 17 are listed for CH_3O and CD_3O where available.

Mode	Normal coordinate	Vibrational symmetry in C_{3v}	JT (vibronic symmetry)	Experimental frequencies (cm^{-1})	
				CH_3O	CD_3O
ν_1	Symmetric stretch	a_1	A_1		
ν_2	H-atom umbrella	a_1	A_1	1367	
ν_3	CO stretch	a_1	A_1	1044	1039
ν_4	Antisymmetric stretch	e	A_1	2810[a]	
			A_2	2810[a]	
			E	2920	
ν_5	H-atom scissoring	e	A_1	1433	
			A_2	1333	
			E	1521	1201
ν_6	CH_3 rock	e	A_1	682	523
			A_2	943	734
			E	1229	920

[a]Because of its high frequency, definitive assignment of the optical spectrum for the antisymmetric stretch modes is not possible.

bonding (p-type) orbital localized largely on the oxygen atom, causing only minimal geometry change upon detachment. The primary change is in the HCH bond angle, implying that the ν_1 and ν_4 modes should not have significant photoelectron activity.

From the theoretical perspective, the methoxy radical has been studied extensively as a prototype of the interaction between the Jahn-Teller effect and spin-orbit coupling (well reviewed by Carter and Cook[22]). Several recent theoretical studies have investigated why the PE spectra are dominated by excitation in non-totally symmetric vibrational modes. Höper *et al.*[23] focused first on explaining the linear and quadratic Jahn-Teller effect in the ground electronic state of methoxy. The authors used multireference configuration interaction (MRCI) calculations to generate potential energy surfaces for the ground states of CH_3O and CD_3O. Based on these surfaces and the Jahn-Teller Hamiltonian, they calculated vibronic frequencies for both radicals. These calculations formed the basis for further work by Schmidt-Klügmann *et al.*[24] describing the effect of the bilinear Jahn-Teller coupling on the spin-orbit splittings by including a spin-orbit coupling term in the Hamiltonian and using the previously determined potential surfaces to recalculate the coupling terms. This work concluded that the bilinear terms, which mix vibrational modes of different symmetries, are essential to a full treatment of the methoxy radical. Schmidt-Klügmann *et al.* used their results to simulate the photoelectron spectral positions and intensities, reproducing the qualitative features only by inclusion of the symmetry-mixing terms. Most recently, higher order (cubic and quartic) Jahn-Teller terms were included in a spin-vibronic model Hamiltonian,[25] providing a higher accuracy than that achieved in the second order simulations of Schmidt-Klügmann *et al.*

TABLE II. Electron affinities determined from previous photoelectron measurements.

Authors (year)	Ref. number	EA(CH_3O) (eV)	EA(CD_3O) (eV)
Engelking *et al.* (1978)	6	1.570±0.022	1.552±0.022
Osborn *et al.* (1998)	7	1.568±0.005	1.551±0.005
Ramond *et al.* (2000)	8	1.572±0.004	1.559±0.004
This work	···	1.5690±0.0019	1.5546±0.0019

By investigating the methoxide anion with SEVI,[3] we expect to resolve many of the features that were not seen in earlier anion PE spectra. In SEVI, relatively slow photoelectrons are imaged onto a position-sensitive detector, yielding a high resolution PE spectrum over a narrow range of electron kinetic energy. This method provides resolution comparable to that of anion zero electron kinetic energy (ZEKE) spectroscopy,[26] i.e., routinely below 1 meV, while offering considerably higher data collection rates in comparison to ZEKE spectroscopy. The SEVI spectra presented here show transitions to vibronic states which were not resolved in earlier PE spectra, including the spin-orbit splitting of the vibronic ground state as well as transitions to previously unobserved modes; these results are compared with recent calculations of the spin-orbit and Jahn-Teller effects in methoxy. Energy-dependent photoelectron angular distributions (PADs) have been recorded for the origin transitions, and the implications of the distributions are discussed. Finally, several hot bands are observed, yielding the first experimental values for some of the anion vibrational frequencies.

II. EXPERIMENT

The SEVI technique has been described in detail previously.[3] A summary, highlighting recent improvements and system specifics, is given here. An overview of the apparatus is shown in Fig. 1. Methoxide (CH_3O^-) and perdeuterated methoxide (CD_3O^-) anions are produced by expand-

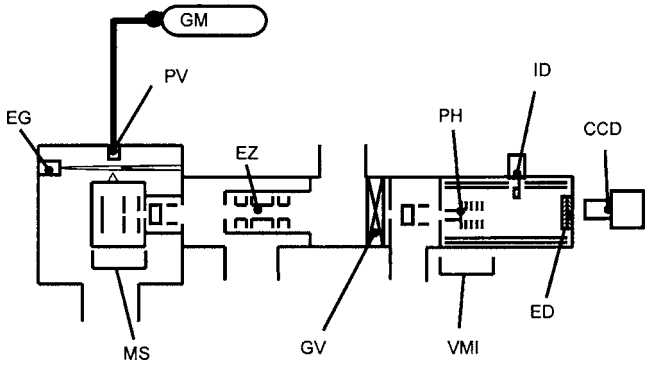

FIG. 1. Modified SEVI apparatus, showing the perpendicular Wiley-McLaren-type mass spectrometer and the pinhole location within the VMI assembly. GM—gas mixture; PV—pulsed valve; EG—electron gun; MS—perpendicular extraction Wiley-McLaren mass spectrometer plates; EZ—Einzel lens; GV—gate valve; VMI—VMI plates and ion gate; PH—3-mm pinhole; ID—retractable ion detector; ED—electron detector; and CCD—charge-coupled device (CCD) array camera.

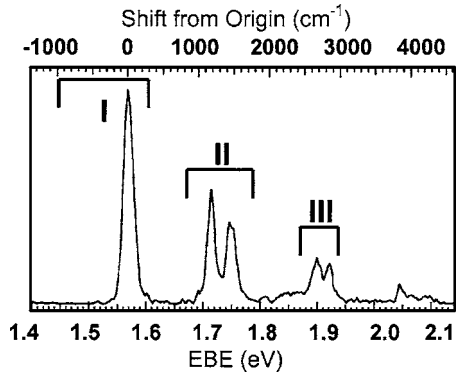

FIG. 2. Photoelectron spectrum of CH_3O^- at 532 nm (18 797 cm^{-1}), taken from Ref. 7. Regions I–III are the sections covered by the SEVI spectra in Figs. 3 and 4.

ing Ne at 50–70 psi (gauge), seeded with approximately 1 torr methanol (CH_3OH) or perdeuterated methanol (CD_3OD), into a vacuum through a pulsed supersonic expansion which is crossed by a pulsed electric discharge stabilized by a 1-keV electron beam. Previous experiments[6] using CH_3OD as a precursor showed that the proton (or deuteron) is removed only from the oxygen atom by this process; no CH_2OH^- is produced. The resulting ions are largely in their ground vibrational and electronic states, although some vibrational excitation can be observed as explained in the discussion below. Ions are extracted perpendicularly into a Wiley-McLaren time-of-flight mass spectrometer ($m/\Delta m \sim 400$) at an ion beam energy of 1250 eV and directed by a series of standard electrostatic optics through a 3-mm pinhole approximately 1.5 m downstream from the mass spectrometer plates. A plate containing a second 3-mm pinhole serves as the repeller plate in our velocity-map imaging (VMI) setup, and is followed by an extraction and then a grounded plate, similar in design to the original VMI experiments of Eppink and Parker.[27] In contrast to our original design, which used pulsed electric fields, all plates are now maintained at a constant negative potential, with the extraction plate held near 70% of the potential on the repeller plate. Because the ion beam translational energy is considerably higher than the repeller potential (1250 V versus at most 350 V), the resulting ion beam expansion due to the dc field is minor and does not affect the electron signal at the voltages used here.

Electron detachment is accomplished with a laser pulse from a 20-Hz Nd:YAG pumped, tunable nanosecond-dye laser that intersects the ion beam between the repeller and extraction plates of the VMI stack. The laser beam is focused by a 40-cm focal length cylindrical lens to a minor diameter of approximately 1 mm along the beam axis. Focusing the laser beam and maintaining consistency in its position are crucial to the improvements in resolution and stability obtained since our original publication. To reduce distortions in our images, which degrade the PE spectral resolution, the electron flight region has been shortened to 50 cm from its original length of 1 m.[3]

Detached electrons are mapped onto a two-dimensional microchannel plate (MCP) detector coupled to a phosphor screen; hits on the screen are collected by a digital camera and sent to a personal computer for analysis. All of the spectra shown here are the result of 50 000–100 000 experimental cycles. The resulting images in velocity space are quadrant symmetrized (preserving any angular information), then converted to a slice through the original three-dimensional PE distribution using an inverse Abel transform. The transformed image is integrated over all angles to yield a photoelectron spectrum in velocity space, which is then transformed into energy space.

The apparatus is calibrated at each pair of repeller and extraction voltages by acquiring a series of PE images of atomic chloride at different electron kinetic energies (eKEs). In the case of atomic spectra, the peak width in energy (ΔE) improves considerably as the repeller plate potential is reduced from 350 to 150 V. At a given voltage, ΔE increases from less than 1 cm^{-1} at the center to as much as 50 cm^{-1} at the edges of the image. Below 150 V, the images become distorted by stray fields, degrading the quality of the transformed images. In the present work the spectral resolution was limited by the anion rotational profiles. The underlying structure could not be resolved even at the lowest imaging voltages. Therefore, all data shown in this paper were obtained using a repeller voltage of 250 V. At this voltage, ΔE for the atomic images is approximately 18 cm^{-1} at eKE $=500$ cm^{-1}, the maximum kinetic energy in the spectra presented here.

III. RESULTS

The PE spectrum of CH_3O^- recorded by Osborn *et al.*[7] at 532 nm is shown in Fig. 2. Regions where SEVI spectra were obtained are labeled in this figure. Figures 3 and 4 show a series of SEVI spectra, each taken close to the threshold of the major peaks seen in Fig. 2. Although the detachment energies used are indicated in each figure caption, the abscissas of the plots are always shown in terms of the electron binding energy (EBE), where

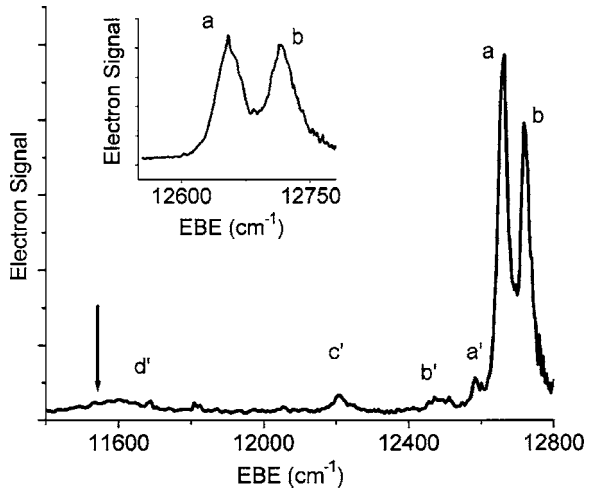

FIG. 3. SEVI spectrum taken near the ground state detachment threshold of CH_3O^- at 12 973.3 cm^{-1}. The inset shows a detail of the band origin. The arrow indicates the location of the ν_6 hot band as determined from the SEP data and the sequence bands to the A_1 and A_2 components in the neutral (see text).

$$EBE = h\nu - \mathrm{eKE}. \quad (1)$$

Here, $h\nu$ is the photon energy and eKE is the measured electron kinetic energy. Although the ground state is present in all images used here, only the near-threshold portion of the spectrum is shown in each panel.

Figure 3 shows the SEVI spectrum corresponding to region I in Fig. 2, using a detachment energy of 12 973.3 cm^{-1}; this region includes the previously assigned vibronic origin of the PE spectrum.[7,8] Peaks a and b (shown in detail in the inset) are well resolved, centered at 12 655 and 12 717 cm^{-1}, with widths of 31 and 38 cm^{-1}, respectively. The conventional PE spectra showed only one broader (100 cm^{-1}) peak in this region. Several peaks are seen at lower EBE (peaks a′–d′) which had not been previously reported. The peak positions found for each image are summarized in Table III.

Figure 4(a) shows the CH_3O spectrum for region II taken at 14 075.9 cm^{-1}. Here, three or four peaks are observed, each 30–40 cm^{-1} wide. The two most intense peaks at 13 888 (c) and 14 174 cm^{-1} (f) agree well with data from the previous PE spectra,[7,8] assigned to the E components of the 6^1 and 5^1 states based on earlier SEP and fluorescence data.[17] Peak d, centered at 14 031 cm^{-1}, had not been observed in previous PE spectra because the instrumental resolution was insufficient to separate the dominant peaks from one another. In addition, a smaller peak may also be present near 14 090 cm^{-1} (labeled e).

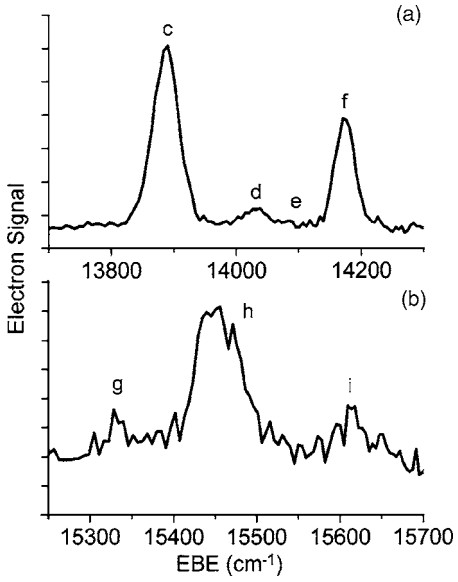

FIG. 4. SEVI spectra of CH_3O^- taken (a) at 14 075.9 and (b) 15 973.1 cm^{-1}.

The spectrum of region III, obtained at 15 973.1 cm^{-1}, is displayed in Fig. 4(b). The most dominant feature (h) is centered around 15 441 cm^{-1}, with an approximate width of 65 cm^{-1}, nearly twice the width of most of the lower EBE peaks; it may well comprise more than one vibronic feature. The same is true of feature i, centered around 15 610 cm^{-1}.

Figure 5 shows the PE spectrum of CD_3O obtained by Osborn *et al.*,[7] taken at 416 nm (24 040 cm^{-1}), again labeled to indicate the SEVI regions shown in greater detail in Figs. 6 and 7. The spectrum in Fig. 6, taken at 12 738.9 cm^{-1} and covering region I in Fig. 5, shows two large peaks: peak a, centered at 12 539 cm^{-1} (31 cm^{-1} wide), and b, at 12 595 cm^{-1} (42 cm^{-1} wide). Several smaller peaks precede the peaks associated with detachment to the vibronic ground state. Table IV summarizes these and the other peak positions determined for CD_3O.

Figure 7(a) shows similar structure in CD_3O to that seen in CH_3O in Fig. 4(a). This spectrum over region II was collected at 14 084.5 cm^{-1}. Again, two major peaks are observed (peaks c and g), with smaller peaks in between the two (peaks d–f). Region III, recorded at a detachment energy of 15 151.5 cm^{-1}, is shown in Fig. 7(b). In contrast to the spectra obtained in CH_3O (but consistent with the previous PE spectra), the features in this portion of the deuterated methoxy radical spectrum are well above the noise level. Although they are irregularly shaped, at least four features are identified; the largest, peak h, is centered at 14 609 cm^{-1}, peaked at 14 600 cm^{-1}, and has a total width of 215 cm^{-1}. The structure seen here is consistent with the previous PE spectra, which showed several irregularly shaped peaks in this portion of the spectrum.

IV. DISCUSSION

A. Region I

The SEVI spectra of the methoxide anion bring to light several features which had not been observed in earlier PE spectra. First, the transition to the vibronic ground state of the methoxy radical has two components rather than the single, broader peak seen in lower resolution spectra. Peaks a and b of Fig. 3, similar in intensity, are split in our spectra by 63 cm^{-1}, in excellent agreement with the 62 cm^{-1} spin-orbit splitting determined by optical spectroscopy directly on the radical,[16] and are assigned to the two spin-orbit components of the vibrational origin, as indicated in Table III. We assign the EAs for CH_3O and CD_3O as the center of the transition to the lower ($^2E_{3/2}$) spin-orbit level. This yields an improved EA for the methoxy radical of 12 655±15 cm^{-1} (1.5690±0.0019 eV, errors based on peak half-width at half

TABLE III. Peak positions and assignments for the SEVI spectra of CH_3O^-. Experimental frequencies are from Ref. 17 (an average of dispersed fluorescence and stimulated emission pumping data). Second-order calculations, which include the bilinear Jahn-Teller, effects are taken from Refs. 24 and 29. Fourth-order calculations are taken from Ref. 23, and also include cubic effects.

Peak	EBE (cm^{-1})	Shift from origin (cm^{-1})	SEP/DF frequency (cm^{-1})	Second-order calculations [fourth-order]	Assignment (vibronic symmetry)
d′	11 597	−1058			6_1^0 and 3_1^0
c′	12 216	−439			$6_1^1(A_1)$
b′	12 482	−173			$6_1^1(A_2)$
a′	12 587	−68			$3_1^1(E)$
a	12 655	0	0		$0_0^0(E)$
b	12 718	63	62	62[a] [65]	$0_0^{0^*}(E)$
c	13 888	1233	1229	1324 [1286]	$6_0^1(E)$
d	14 031	1376	1367	1411 [1391]	$2_0^1(E)$
e	14 084	1429	1414	1449 [1425]	$2_0^{1^*}(E)$
f	14 174	1519	1521	1581 [1526]	$5_0^1(E)$
g	15 340	2685			
h	15 441	2786	2761	N/A	$5_0^2(E)$
i	15 610	2955	2920	N/A[b] [2972]	$4_0^1(E)$

[a]The value of the spin-orbit splitting parameter was selected to reproduce the experimental value.
[b]In the calculations by Schmidt-Klügmann *et al.* ν_4 and ν_1 are not included.

maximum), well within the error bars of both Osborn *et al.* and Ramond *et al.* Note that since the spin-orbit states were not resolved in previous PE spectra, the EAs determined from those spectra should be slightly high, as they were taken to be the center of the broad feature assigned to the ground state.

Analysis of the region I peaks in the CD_3O spectrum yields similar conclusions: the spin-orbit splitting determined using peaks a and b in Fig. 4 is 55 cm^{-1} (cf. 56 cm^{-1} from emission experiments[16]), with an electron affinity of 12 539±15 cm^{-1} (1.5546±0.0019 eV). The EAs determined by this work are shown alongside the previous values in Table II for comparison. The CD_3O spectrum shows the same widths seen in the spectrum of CH_3O, indicating approximately equal rotational temperatures.

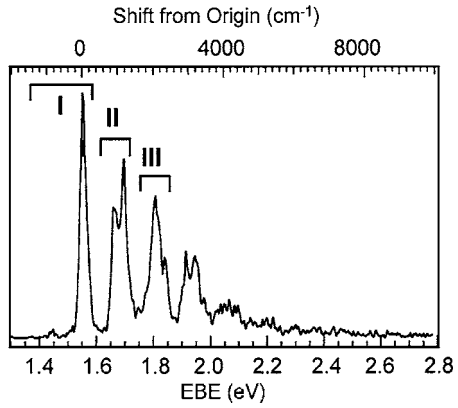

FIG. 5. Photoelectron spectrum of CD_3O^- at 416 nm (12 794 cm^{-1}), taken from Ref. 7. Regions I–III are the sections covered by the SEVI spectra in Figs. 6 and 7.

Based on the assignments above for the ground state, Table III (Table IV for CD_3O) shows the energies of all transitions relative to the ground spin-orbit state. Where assignments can be made, they are indicated in the tables, along with the corresponding SEP frequencies.[17] The calculated results from both Schmidt-Klügmann *et al.*[24] and Marenich and Boggs[25] are also included where available.

Spectra taken closer to threshold or at greater magnification (by reducing the VMI repeller voltage) did not improve the peak width of at least 30 cm^{-1} for all peaks in regions I and II. As this value is considerably larger than the resolution of our instrument, we conclude that the width is

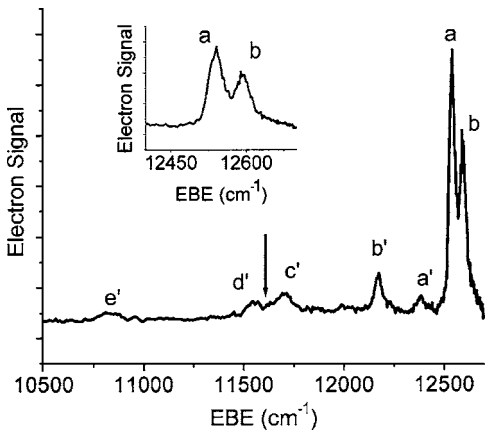

FIG. 6. SEVI spectrum taken near the ground state detachment threshold of CD_3O^-, taken at 12 738.9 cm^{-1}. The inset shows the detail of the band origin. The arrow indicates the location of the ν_6 hot band as determined from the SEP data and the sequence bands to the A_1 and A_2 components in the neutral.

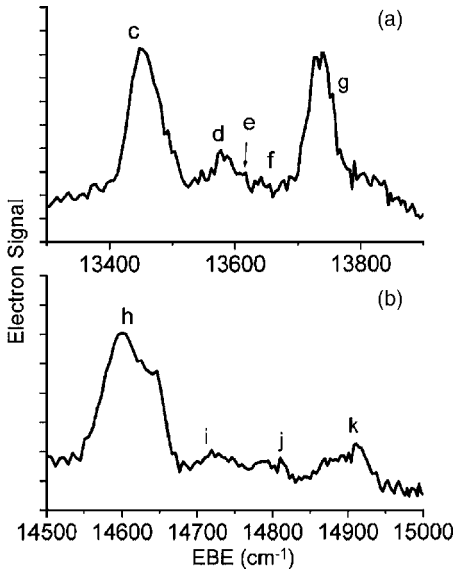

FIG. 7. SEVI spectra for CD_3O^- taken (a) at 14 084.5 and (b) 15 151.5 cm^{-1}.

due to rotational excitation of the anion, leading to a distribution in the detachment spectrum. Although rotational selection rules for PE spectroscopy are more involved than in optical spectroscopy, the line shapes can be simulated approximately by treating the anion and neutral as rigid prolate tops, allowing $\Delta J=0,\pm1$ and $\Delta K=0,\pm1$ and neglecting nuclear and electronic spins. We estimate the rotational temperature in our experiments to be 30–40 K.

B. Region II

Region II comprises transitions to vibrationally excited states of CH_3O and CD_3O. Because the degeneracy of the ground electronic state ($\tilde{X}\,^2E$) is lifted by the Jahn-Teller interaction, the non-totally symmetric modes (all of which belong to the e vibrational representation) are split into vibronic A_1, A_2, and E components within C_{3v} symmetry. In both optical and PE spectroscopies, the coupling between the vibrational angular momentum (l) and the Jahn-Teller quantum number, $j\equiv l\pm\frac{1}{2}\Lambda$ (Λ is the projection of l onto the principal rotational axis), dictates the allowed transitions.[28] To first order, the selection rules here are just as for transitions between degenerate and nondegenerate components: the allowed transitions must obey $l'=j\pm\frac{1}{2}$, where l' is the vibrational angular momentum of the nondegenerate state (in this case, the anion). Thus transitions to the A_1 and A_2 vibronic states ($j=3/2$) in the ν_5 and ν_6 modes of the radical are forbidden to first order from the ground state of the anion, while transitions to the E vibronic components ($j=1/2$) are allowed.

TABLE IV. Peak positions and assignments for the SEVI spectra of CD_3O^-: References are as in Table III.

Peak	EBE (cm^{-1})	Shift from origin (cm^{-1})	SEP/DF frequency (cm^{-1})	Second order calculations	Assignment
e′	10 829	−1710			$4_1^0,3_2^0,3_1^06_1^0$
d′	11 547	−992			$6_1^0,3_1^0,5_1^0$
c′	11 700	−839			$6_1^0,3_1^0,5_1^0$
b′	12 171	−368			$6_1^1(A_1)$
a′	12 384	−155			$6_1^1(A_2)$
a	12 539	0	0		$0_0^0(E)$
b	12 594	55	54	56	$0_0^{0^*}(E)$
c	13 448	909	920	942	$6_0^1(E)$
d	13 575	1036	1039	1039	$3_0^1(E)$
e	13 617	1078	N/A	1059	$3_0^{1^*}(E)$
f	13 641	1102	1121	1141	$2_0^{1^*}(E)$
g	13 734	1195	1201	1212	$5_0^1(E)$
h	14 609	2070	N/A	N/A	$5_0^2(E)$
i	14 728	2189			$4_0^1(E)$
j	14 794	2255			
k	14 896	2357			

The transitions shown in Figs. 4(a) (peaks c and f) and 7(a) (peaks c and g) are assigned to the E component of the fundamental frequencies of the ν_5 and ν_6 modes, as indicated in Tables III and IV. The positions of these peaks are consistent with previous assignments of the SEP spectra.[18] Peak d in Fig. 4 is therefore assigned to the umbrella mode (ν_2) in CH_3O, yielding a vibrational frequency that is in close agreement with the SEP data. The very small shoulder, peak e, is separated from the ν_2 peak by 53 cm^{-1}. The SEP experiments determine the spin-orbit splitting of the ν_2 mode to be 47 cm^{-1}. We therefore tentatively assign peak e to the spin-orbit excited state of the ν_2 fundamental. The small size of the shoulder relative to the noise level makes it difficult to make a final assignment.

In the CD_3O spectrum [Fig. 7(a)], there are two and possibly three peaks between the ν_5 and ν_6 peaks c and g. The isotope effect in the umbrella, scissor, and CH_3 rock modes is considerable, owing to the large amplitude motion of the hydrogen atoms in these modes. To complicate the situation, the CO stretch frequency is changed only slightly upon deuteration, leaving all four of the ν_2, ν_3, ν_5, and ν_6 modes in the 950–1200 cm^{-1} range. We assign peaks d and e to the ν_2 and ν_3 modes, again by comparison with the established SEP data. However, the proper assignment of these peaks to the actual normal modes is less straightforward. Foster *et al.*[11] assigned the lower frequency mode to the CO stretch and the higher frequency mode to the umbrella mode. The rovibronic structural studies allowed the assignment of vibronic features to specific symmetry components based on their rotational signatures, but transitions with similar rotational profiles cannot be distinguished in this manner. The lower frequency mode is considerably more intense in our spectra, and, since the CO stretch was not even observed in CH_3O (although it should be well separated from the other peaks and within the range of our images), we assign peak d to the umbrella mode (with peak e tentatively assigned to its spin-orbit excited counterpart), and peak f to CO stretching. With this assignment, which differs from that of Foster *et al.*, the normal modes associated with the ν_2 and ν_3 labels are switched in CD_3O compared to CH_3O because the energetic ordering of the vibrational states changes.

Some smaller features from the conventional PE spectra in this region are not observed in the SEVI spectrum. The unobserved features are those found previously[8] to have dif-

ferent angular distributions from the peaks observed here and were assigned to transitions to components with A_1 vibronic symmetry. To determine angular distributions, Osborn *et al.* and Ramond *et al.* rotated the laser polarization to collect at a different scattering angle (θ) relative to the laser polarization. The E-symmetry peaks showed a $\sin^2(\theta)$ distribution, while the A_1-symmetry peaks had a $\cos^2(\theta)$ distribution. Given that the anisotropy of the ground state transitions has nearly reached its high eKE value (as determined by Ramond *et al.*[8]) by the highest energy detachment used here (see Sec. IV E below), we might expect to see the transitions to A_1 components seen in previous PE spectra. Even in the spectra taken at 635 nm, more than 2400 cm^{-1} above the threshold for the A_1 component, no transition is visible. However, even collecting along the maximum of the A_1-symmetry peaks, with the intensity of the E-symmetry peaks at a minimum, the A_1-symmetry peaks in the spectrum of Ramond *et al.* are tiny by comparison. Thus, because we integrate over all angles for all peaks, the features would be considerably smaller than indicated by previous PAD studies.

As for the spin-orbit interaction, our spectra do not show spin-orbit coupling in the ν_5 and ν_6 modes for either CH_3O or CD_3O. Jahn-Teller coupling may reduce the spin-orbit splitting below the widths of the rotational contours in our spectra. Indeed, the calculations by Schmidt-Klügmann *et al.*[24] indicate that the spin-orbit levels are split by at most 19 cm^{-1} in these states, and less than 10 cm^{-1} in some cases (although no experimental information is currently available). Our improved resolution does, however, allow us to confirm the predictions made by Schmidt-Klügmann *et al.* regarding the presence of additional states in the PE spectrum between the ν_6 and ν_5 modes. The best simulations of the PE spectra from that work first calculate the anion geometries and frequencies, then determine the spectral intensities using a Poisson distribution in the change of the normal modes upon electron detachment. Only by including the bilinear coupling terms (which mix the ν_2, ν_3, ν_5, and ν_6 modes with one another) are the predicted intensities of the ν_2 and ν_3 modes reduced below that of the ν_5 and ν_6 peaks in the photoelectron spectrum. Our verification that the umbrella modes (and possibly the CO stretch mode in CD_3O) are present, though weak, supports inclusion of the bilinear terms in the spin-vibronic Hamiltonian as being essential to an adequate description of the Jahn-Teller effect in the methoxy radical.

C. Region III

Next, the states shown in Figs. 4(b) and 7(b) are considered. The features observed in these regions are more than 2700 cm^{-1} (2000 cm^{-1}) above the detachment threshold for CH_3O (CD_3O). As mentioned above, the irregularly shaped features in these regions are indicative of overlapped transitions, which could be combination bands between the ν_5 and ν_6 modes. The peak positions are consistent with the recent PE spectra,[7,8] with only slightly different intensities than in those spectra.

Unfortunately, the previously reported optical spectra are congested in this region, making definitive assignment impossible. Based on the SEP data available for this region, we may suggest some (but not necessarily all) possible assignments for these peaks. First, it is possible that one of the peaks in this region is due to detachment to the ν_4 mode. The SEP frequencies assigned to this mode for CH_3O are in the same general vicinity as the peaks in Fig. 4(b). Experimental values for the ν_4 mode in perdeuterated methoxy could not be found. Previous PE papers on methoxy radical have eliminated the asymmetric stretch as a possible carrier of PE activity based on negligible Franck-Condon overlap between the anion ground state and the first excited state in the radical. However, the Jahn-Teller effect in methoxy may mix the modes (as with the modes discussed in the previous section), allowing PE activity to some extent. Second, SEP experiments assign the 5_0^2 transition to 2761 cm^{-1} in CH_3O, within the broad feature h of Fig. 4(b). Furthermore, overtones and combination bands between the ν_5 and ν_6 modes are also expected within this range for both CH_3O and CD_3O. These may also account for the highest EBE peaks observed in both radicals.

TABLE V. Calculated vibrational frequencies for the anions CH_3O^- and CD_3O^-. All values are taken from work by Schmidt-Klügmann *et al.* (Ref. 24 and 29), and are calculated at the CCSD(T) level using the aug-cc-pVTZ basis with 161 contracted Gaussian-type orbitals. Where available, the frequencies determined in this work are also listed. For spectral features which could not be uniquely identified, the same frequency is listed more than once.

	CH_3O^- frequencies (cm^{-1})		CD_3O^- frequencies (cm^{-1})	
Mode	CCSD(T)	SEVI	CCSD(T)	SEVI
ν_1	2650		1890	
ν_2	1452		1169	
ν_3	1129	1113	1030	839 or 992
ν_4	2559		1887	1710
ν_5	1454		1064	839 or 992
ν_6	1161	1120	902	944

D. Anion excitation

Below the EA, transitions from vibrationally excited states of the anion are seen. The original PE spectrum[6] did show one similar hot band 1075 cm^{-1} below the origin which was assigned to the umbrella mode (based on the ν_2 progression assigned to their spectrum). A reassessment of the hot bands is required, given the change in interpretation of the vibrational structure in the radical. Anion vibrational frequencies recently obtained by Schmidt-Klügmann *et al.*[24,29] using coupled-cluster methods CCSD(T) with Dunning's augmented correlation-consistent basis with triple zeta (aug-cc-pVTZ) are shown in Table V. These calculations are used as guidelines for the assignment of the peaks below the vibronic origin. As mentioned above, transitions to the A_1 and A_2 components of the radical are forbidden from the ground state of the anion. Vibrational excitation in the degenerate modes of the anion creates vibrational angular momentum, allowing anion to radical transitions which would otherwise be forbidden to first order.

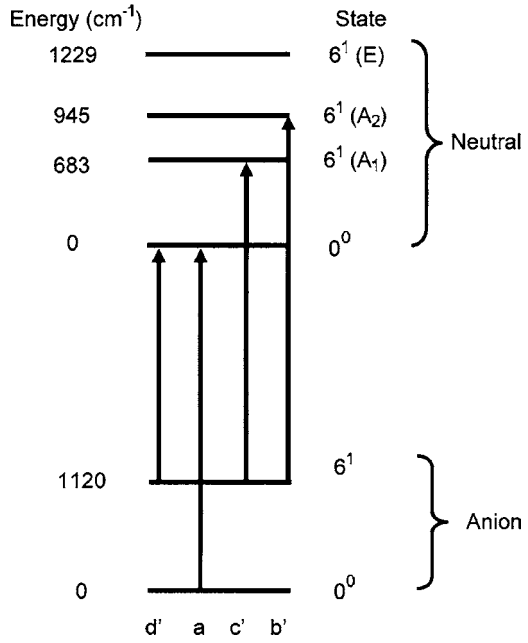

FIG. 8. Schematic of the various hot bands and sequence bands with the ν_6 manifolds of the methoxide anion (CH_3O^-) and methoxy radical. The arrows connecting pairs of states are labeled underneath the manifold according to the scheme in Fig. 4(b) and Table III.

In the CH_3O^- spectrum (Fig. 3), the largest frequency hot band, 1058 cm^{-1} below the origin (feature d′), overlaps with the calculated frequencies for the ν_6 (CH_3 rock) and ν_3 (CO stretch) modes, the lowest frequency modes available. In CD_3O^- (Fig. 6), there is a broad, structured feature with peak centers c′ and d′ identified in Table IV that are 839 and 992 cm^{-1} from the origin, and which lie closest to the calculated frequencies for the ν_6 and ν_3 modes, respectively, although the ν_5 mode also is in range. In both cases, the hot band features are quite broad as they represent transitions to both spin-orbit states of the radical from at least two different energy levels in the anion.

Further insight into the anion frequencies and assignments is gained from peaks a′–c′ in Fig. 3 and peaks a′ and b′ in Fig. 6. As seen in Tables III and IV, these peaks are too close to the origin to represent $\Delta v=-1$ hot band transitions, and instead are more likely to be sequence bands between vibrationally excited levels of the anion and radical. In the SEP experiments[17] on CH_3O, transitions assigned to the $6^1(A_1)$ and $6^1(A_2)$ levels lie 683 and 945 cm^{-1} from the spin-vibronic ground state and are thus separated by 262 cm^{-1}. This spacing is very similar to that between peaks b′ and c′ (266 cm^{-1}), suggesting these peaks be assigned to transitions from the singly excited ν_6 state of the anion to the A_1 and A_2 vibronic components of the same mode in the neutral (the 6_1^1 transitions; see Fig. 8), as indicated in Table III. Adding 683 and 945 cm^{-1} to the frequencies below origin of peaks c′ and b′ yields 1122 and 1118 cm^{-1}, respectively, for the ν_6 fundamental in the anion, which, as shown in Fig. 3, lies well within the broad envelope of peak d′. Hence, this assignment yields overall consistency between the SEVI and SEP spectra. Although accessing the E component from the singly excited anion would also be possible, the transition would lie approximately 150 cm^{-1} above the origin, still obscured by the spin-orbit excited state of the radical ground state transition.

Peak a′ is assigned to the 3_1^1 sequence band. Here, the SEP frequency for the fundamental is 1045 cm^{-1}, and the anion frequency is larger by 68 cm^{-1} (the frequency difference between peaks a′ and a) yielding an anion frequency of 1113 cm^{-1}, also in reasonable agreement with both the calculations and feature d′ in Fig. 3. Figure 8 illustrates the assignments of some of the observed hot and sequence bands.

By similar reasoning, peaks a′ and b′ in Fig. 6 appear to be $6_1^1(A_2)$ and $6_1^1(A_1)$ sequence bands in CD_3O. The splitting between these two features, 213 cm^{-1}, is close to the splitting of the A_1 and A_2 components (at 584 and 780 cm^{-1}, respectively) as assigned in the SEP spectra.[18] Assuming this assignment for peaks a′ and b′ yields anion ν_6 frequencies of 952 and 935 cm^{-1}, the 6_1^0 transition corresponding to the average of these values, 944 cm^{-1}, is shown in Fig. 6. This transition lies in the middle of the small feature that includes peaks c′ and d′, which are, as mentioned above, likely be a combination of hot bands with associated spin-orbit splitting. We hesitate to put forward a more definitive assignment of this cluster of peaks, other than to say that it includes the 6_1^0 transition and may also contain the 3_1^0 and 5_1^0 transitions. Additional data are needed on the vibrational frequencies for a full assignment of the methoxide anion.

The broad feature e′ (1710 cm^{-1} below the origin) could be an unresolved pair of the 3_2^0 and $3_1^0 6_1^0$ transitions. The 6_2^0 transition is also energetically possible, but this would require violation of the selection rules mentioned above, and, since no peaks are observed at the expected frequencies for the corresponding (allowed) sequence bands, this possibility is rejected. Alternatively, the ν_1 and ν_4 modes are predicted to lie near this frequency. As explained above, these modes should not be PE active. Based on arguments for the assignment to the ν_4 mode given above, however, feature e′ may have some contributions from ν_4.

E. Photoelectron angular distributions

The SEVI experiment also yields photoelectron angular distributions (PAD) as a function of photon energy. In a photodetachment experiment, the differential cross section, $d\sigma/d\Omega$, is described by[30]

$$\frac{d\sigma}{d\Omega}=\frac{\sigma_{\text{total}}}{4\pi}\left(1+\beta(\text{eKE})\left(\frac{3}{2}\cos^2(\theta)-\frac{1}{2}\right)\right), \tag{2}$$

where σ_{total} is the total photodetachment cross section, β(eKE) is the anisotropy parameter used to characterize the angular distribution, and θ is the angle between the directions of PE ejection and the polarization vector of the incident radiation. We obtain β(eKE) for the 0_0^0 transitions by analysis of the images at several photon energies; these values are plotted in Fig. 9. For both isotopomers, β(eKE) starts around −0.3 at low eKE, remains relatively constant for ~2000 cm^{-1}, then rises to the value of −0.9 at the highest eKE (not plotted in Fig. 9), in agreement with the value determined by Ramond *et al.*[8] by changing the polarization.

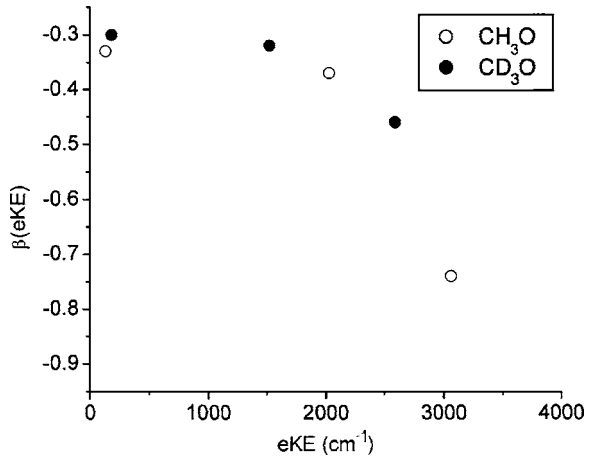

FIG. 9. Plot of β(eKE) for the ground vibronic state transitions in CH_3O (open circles) and CD_3O (closed circles).

Near threshold, the photodetachment cross section, σ, is described by the Wigner threshold law,[31]

$$\sigma \propto (\mathrm{eKE})^{\ell+1/2}, \tag{3}$$

where ℓ is the angular momentum of the scattered electron partial wave. As a result, true anion ZEKE experiments[26] are feasible only when s-wave ($\ell=0$) detachment dominates near threshold, because otherwise the photodetachment cross section is too small for the experiment to be feasible. This condition is relaxed somewhat in SEVI experiments which do not, in general, need to be performed right at the threshold for a particular photodetachment transition. The present case corresponds mainly to photodetachment from a localized p-type orbital, which results in predominantly s-wave detachment ($\ell=0$; isotropic PAD with $\beta=0$) near threshold, and gradually more contributions from d-wave detachment with increasing eKE. Interference between s and d waves yields a $\sin^2\theta$ PAD, with $\beta=-1$. These trends are clearly seen in Fig. 9, which shows the evolution from a nearly isotropic to nearly perpendicular PAD with increasing eKE.

V. CONCLUSIONS

Higher resolution photodetachment spectra of methoxide and perdeuterated methoxide provide improved electron affinities for the corresponding radicals and have revealed new information which answers a number of questions arising from the two most recent PE spectra for these species. The ground state spin-orbit splitting is resolved and is consistent with previous work on this aspect of the methoxy radical. Photoelectron angular distributions as a function of electron kinetic energy support the conclusion of previous calculations that the detached electron resides in a localized p-type orbital in the anion. The SEVI spectra may show some splitting in the totally symmetric modes, but none in the non-totally symmetric ones, owing to the reduced spin-orbit interactions as vibrational excitation progresses in these Jahn-Teller active modes. Peaks unobserved by previous PE studies are detected and assigned to the umbrella mode in CH_3O and to the umbrella and CO stretch modes in CD_3O (in conjunction with SEP studies), supporting theoretical indications that the bilinear terms in the spin-vibronic Hamiltonian are crucial to an adequate description of the methoxy radical. In addition to this new information regarding the radical, vibrational hot bands and sequence bands are observed at EBE lower than the origin, providing some insight into the frequencies of the methoxide anion, a species which has not yet been studied in the gas phase.

ACKNOWLEDGMENTS

This work is supported by the Air Force Office of Scientific Research under Grant No. F49620-03-1-0085. The authors wish to thank Professor H. Köppel for useful and enthusiastic exchanges regarding his calculations.

[1] K. L. Demerjian, J. A. Kerr, and J. G. Calvert, Adv. Environ. Sci. Technol. **4**, 1 (1974).
[2] J. Heicklen, *Atmospheric Chemistry* (Academic, New York, 1976).
[3] A. Osterwalder, M. J. Nee, J. Zhou, and D. M. Neumark, J. Chem. Phys. **121**, 6317 (2004).
[4] D. W. Style and J. C. Ward, Trans. Faraday Soc. **49**, 999 (1953).
[5] H. R. Wendt and H. E. Hunziker, J. Chem. Phys. **71**, 5202 (1979).
[6] P. C. Engelking, G. B. Ellison, and W. C. Lineberger, J. Chem. Phys. **69**, 1826 (1978).
[7] D. L. Osborn, D. J. Leahy, E. H. Kim, E. de Beer, and D. M. Neumark, Chem. Phys. Lett. **292**, 651 (1998).
[8] T. M. Ramond, G. E. Davico, R. L. Schwartz, and W. C. Lineberger, J. Chem. Phys. **112**, 1158 (2000).
[9] J.-X. Han, Y. G. Utkin, H.-B. Chen, L. A. Burns, and R. F. Curl, J. Chem. Phys. **117**, 6538 (2002).
[10] D. E. Powers, J. B. Hopkins, and R. E. Smalley, J. Phys. Chem. **85**, 2711 (1981).
[11] S. C. Foster, P. Misra, T.-Y. D. Lin, C. P. Damo, C. C. Carter, and T. A. Miller, J. Phys. Chem. **92**, 5914 (1988).
[12] S. C. Foster and T. A. Miller, J. Phys. Chem. **93**, 5986 (1989).
[13] X. Liu, C. P. Damo, T.-Y. D. Lin, S. C. Foster, P. Misra, L. Yu, and T. A. Miller, J. Phys. Chem. **93**, 2266 (1989).
[14] Y.-Y. Lee, G.-H. Wann, and Y.-P. Lee, J. Chem. Phys. **99**, 9465 (1993).
[15] P. G. Carrick, S. D. Brossard, and P. C. Engelking, J. Chem. Phys. **83**, 1995 (1985).
[16] S. D. Brossard, P. G. Carrick, E. L. Chappell, S. C. Hulegaard, and P. C. Engelking, J. Chem. Phys. **84**, 2459 (1986).
[17] F. Temps (private communication).
[18] A. Geers, J. Kappert, F. Temps, and T. J. Sears, J. Chem. Phys. **98**, 4297 (1993).
[19] D. L. Osborn, D. J. Leahy, E. M. Ross, and D. M. Neumark, Chem. Phys. Lett. **235**, 484 (1995).
[20] D. L. Osborn, D. J. Leahy, and D. M. Neumark, J. Phys. Chem. A **101**, 6583 (1997).
[21] D. R. Yarkony, H. F. Schaeffer III, and S. Rothenberg, J. Am. Chem. Soc. **96**, 656 (1974).
[22] J. T. Carter and D. B. Cook, J. Mol. Struct.: THEOCHEM **251**, 111 (1991).
[23] U. Höper, P. Botschwina, and H. Köppel, J. Chem. Phys. **112**, 4132 (2000).
[24] J. Schmidt-Klügmann, H. Köppel, S. Schmatz, and P. Botschwina, Chem. Phys. Lett. **369**, 21 (2003).
[25] A. V. Marenich and J. E. Boggs, Chem. Phys. Lett. **404**, 351 (2005).
[26] T. N. Kitsopoulos, I. M. Waller, J. G. Loeser, and D. M. Neumark, Chem. Phys. Lett. **159**, 300 (1989).
[27] A. T. J. B. Eppink and D. H. Parker, Rev. Sci. Instrum. **68**, 3477 (1997).
[28] H. C. Longuet-Higgins, U. Öpik, M. H. L. Pryce, and R. A. Sack, Proc. R. Soc. London, Ser. A **244**, 1 (1958).
[29] H. Köppel (private communication).
[30] J. Cooper and R. N. Zare, J. Chem. Phys. **48**, 942 (1968).
[31] E. P. Wigner, Phys. Rev. **73**, 1002 (1948).